Journal of Applied Fluid Mechanics, Vol. 16, No. 9, pp. 1742-1751, 2023.
Available online at www.jafmonline.net, ISSN 1735-3572, EISSN 1735-3645.
https://doi.org/10.47176/jafm.16.09.1752

Design and Optimization of Online Dynamic Mixer and Its Performance Analysis

Y. W. Zheng[1], J. K. Wang[†1,2], J. G. Sun[1] and C. Y. Wang[1]

[1] *Tianjin Key Laboratory of Integrated Design and On-line Monitoring for Light Industry & Food Machinery and Equipment, Tianjin International Joint Research and Development Center of Low-carbon Green Process Equipment, College of Mechanical Engineering, Tianjin University of Science and Technology, Hexi District, Tianjin,300202, P.R. China*
[2] *Tianjin DTH Machinery Equipment Co., Binhai New District, Tianjin, 300480, P.R. China*

†*Corresponding Author Email: wangjk@tust.edu.cn*

ABSTRACT

In this study, a dynamic mixer was designed to mix polymer melts online during extrusion, and the flow of a polymer melt in a mixer was simulated using Polyflow software. The Orthogonal experiment was conducted to analyze the effects of three geometrical parameters (i.e. the length of entrance zone (L_i), the gap between the rotor and wall (g), and the diameter of cone-shaped rotor (d_2)) on mixing properties of a dynamic mixer. The L_i, g, and d_2 were optimized for the minimum product of segregation scale (S) and power consumption (P). Finally, the mixing properties of the dynamic mixer were compared with those of SK and SX static mixers. The results indicated that among the above-mentioned three parameters, the g was the most important parameter influencing S, and $S{\cdot}P$. The minimum $S{\cdot}P$ of 1059 μm·W was obtained when the L_i was 16 mm, the g was 1 mm, and the d_2 was 24 mm. The S decreased with the increase of the rotation speed from 120 to 360 r/min, and increased with the increase of the flow rate from 15 to 45 mL/min. However, the P increased with the increase of both the rotation speed and flow rate. The maximum shear rate of the melt in the dynamic mixer was observed in the mixing zone, which was mainly affected by the rotation speed rather than the flow rate. To achieve the S of the same size, the length of the dynamic mixer was the shortest, and that of the SK static mixer was the longest. Moreover, to acquire the S of the same size, the dynamic mixer required the largest P, the SX static mixer needed a smaller P, and the SK static mixer required the minimum P.

Article History

Received January 10, 2023
Revised March 31, 2023
Accepted April 11, 2023
Available online July 1, 2023

Keywords:

Mixer
Numerical simulation
Parameter optimization
Power consumption
Segregation scale

1. INTRODUCTION

Melt mixing is an important operation unit for polymer processing machinery. To produce high-performance products, uniform distributions of materials and temperatures are needed which can be provided by well mixing (Eriksson et al., 2020; Chen et al., 2021).

In extrusion molding, the mixing is mostly performed by the screw during melt conveying, compressing, and plasticizing. In the last years, many investigations have been carried out regarding mixing performance and its influence on the properties of products (Carcia et al., 2018). Because of the high efficiency and low cost, numerical methods have been employed to conduct many of these studies. Varga et al. (2020) used the value of mixed volume around the screws to quantify the mixing efficiency, based on which they analyzed the effects of leaf diameter, pitch, and angular velocity on the mixing efficiency. Bauer and Khinast (2022) examined mixing barriers in a twin screw extruder using a numerical method. They compared results obtained through different screw geometries, and found that the order of mixing performance of various twin screw types was mixing > kneading > conveying. Connelly and Kokine (2007) scrutinized the mixing performance of single and twin screw extruders using a numerical method. Via comparing the segregation scale (S) of dough in mixers, they found that the twin screw mixer had obvious advantages over the single screw mixer at the initial stage, but after ten revolutions, the advantages disappeared. The smallest value of about 0.1 mm was found for S in their work. Robinson and Cleary (2019) investigated the effects of screw pitch, knead block stagger angle, gap size, and filling level on the mixing behaviors by using the

Nomenclature

D_i	inlet diameter	S	segregation scale
D_o	outlet diameter	σ^2	variance
d_i	diameter of shaft in the entrance zone	P	power consumption
d_2	diameter of cone-shape rotor	Δp	pressure drop
g	gap between the rotor and wall	T	torque
L_i	length of entrance zone	$S{\cdot}P$	the product of segregation scale and power consumption
L_m	length of mixing zone	Pr_1	inlet position of dynamic mixer
L_o	length of exit zone	Pr_2	inlet position of mixing zone
T_t	temperature	Pr_3	outlet position of mixing zone
N	power law index	Pr_4	outlet position of dynamic mixer
W	power unit, watt		

lagrangian method. The results revealed that the screw pitch and gap size were positively correlated to the mixing rate, and the mixing rate was the largest with the block angle of 30º and filling level of 50%. Jian et al. (2018) designed a novel single screw with a torsion element and compared its mixing effect with a conventional screw using Computational Fluid Dynamics (CFD). They found that the novel screw had a smaller *S* and distribution index, and a higher mixing efficiency, especially with torsion elements arranged in a decentralized way. Xu et al. (2018) developed a novel extrusion system with a corotating nontwin screw, and simulated the melt flow patterns and mixing dynamics in the novel nontwin and conventional twin screw. The results demonstrated that the nontwin screw had better distributive and dispersive mixing capabilities than the conventional twin screw. Marschik et al. (2019) examined the pumping and mixing capabilities of block-head mixers by simulating 3D non-Newtonian flow in the mixing screw. Three geometrical parameters (i.e. the number of flights, the number of blocks, and the stagger angle between the blocks) were chosen to study their influences on the mixing effect, pressure consumption, and energy dissipation. They employed the residence time distribution functions, kinematic stretching parameters, and *S* to characterize the distributive mixing. They also utilized the mixing index and shear stress to describe dispersive mixing. They found that the cross-sectional and axial mixing capability was almost equal for all block-head mixers under consideration. The increase in the number of flights enhanced the mixing performance but increased pressure consumption and energy dissipation. Liu and Zhu (2019) reported a new method to characterize the chaotic mixing effect for the single screw extruder with a perturbation baffle using the Finite Element Method (FEM). Through analysis of the effects of baffle width and height on the manifold structures in the flow dynamics, it was found that the homoclinic point of the manifold structure resulted in chaotic mixing, and the increase in the height of the baffle led to an increase in mixing efficiency. Cai et al. (2019) investigated the flow pattern of particles and the mixing performance of the double-screw conical mixer. They found that the best mixing performance and the lowest power consumption could be procured by reasonably selecting the diameter ratio of the particles and the rotation ratio of the mixer. As mentioned above, although a lot of investigations have been performed about the mixing mechanism of the screw, how to improve the mixing effect and save energy is still a research topic worthy of further study.

Another method to enhance mixing performance is installing a static mixer downstream of the screw. Through supercritical carbon dioxide injection, Common et al. (2014) scrutinized the effect of a static mixer on the melt flow behavior in a single screw extruder. It was found that the static mixer improved mixing by enhancing dispersion, and a more homogeneous porous structure was achieved while using static mixers between the screw tip and die. Rochman and Zahra (2018) developed a mixing nozzle with static mixers in the injection molding of thermoset elastomer. Through experiments, it was observed that the curing time was reduced by 10 s, and the molded parts with better homogeneity and properties were obtained using the mixing nozzle. Carolina et al. (2020) designed a continuous chaotic printing process by using the printhead containing static mixers. By selecting the number of mixing elements and diameter of the printhead, the multilayered micro- or nanostructure was attained in the extruded fibers. Compared with the normal printing process, the dimension of the microstructure was scaled down by 3 orders of magnitude to the nanoscale level (approximating 150 nm). Lin and Chang (2021) placed a static mixer in the runner in the injection molding process to solve the problem of temperature imbalance. By optimizing four geometrical parameters of the static mixer, the maximum temperature uniformity was accomplished during the injection. Talhaoui et al. (2020) developed a novel static mixer called overlapped static mixer, and examined the flow pattern and mixing behavior of fluid in both the general and overlapped static mixer by using CFD. By comparing the pressure drop and intensity of segregation of two types of static mixers, they found that the improvement of the mixing effect was usually accompanied by the increase of pressure drop and length of static mixers.

Past investigations and studies suggest that the quality of mixing directly affects the properties of the final product. Most mixing operations are performed by specially designed screw mixing elements or static mixers. For the screw mixing element, the mixing performance can be adjusted by changing the rotation speed of the screw during production. For the static mixer, the adjustment of mixing performance is required to change the length of the static mixer, which in turn requires stopping production and adjusting the equipment. From this point of view, the use of screw mixing elements

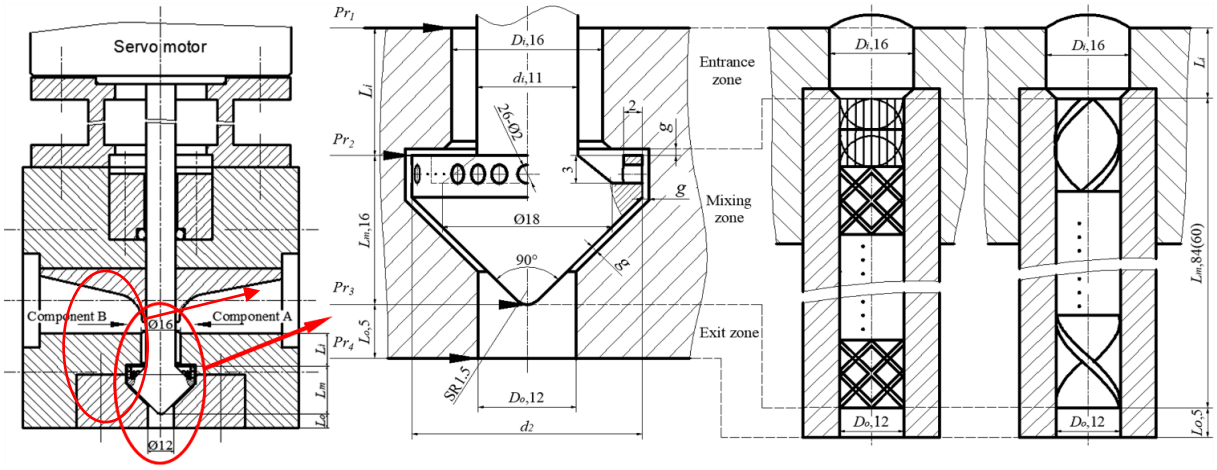

(a) (b) (c) (d)

Fig. 1. (a) the assembly drawing of the dynamic mixer, (b) the detailed view of dynamic mixer, (c) SX static mixer, and (d) SK static mixer.

is more convenient. However, the improvement in mixing performance is usually accompanied by an increase in energy consumption (Talhaoui et al., 2020). Thus, it is important to calculate and reduce the energy consumption in the mixing process. For the static mixer, the energy consumed by mixing can be calculated by pressure drop and flow rate. But for screw, which has other functions such as conveying, compressing, and plasticizing, it is difficult to separate the energy consumption by mixing from the whole energy consumption. Therefore, completed studies similar to our research can rarely be found in past investigations.

We designed a dynamic mixer to perform the mixing operation. Based on the numerical simulation and Orthogonal experiment, the three main geometrical parameters (i.e. length of entrance zone (L_i), the gap between the rotor and wall (g), and the diameter of cone-shaped rotor (d_2)) were optimized for the minimum product of S and power consumption (P). Besides, the effects of the flow rate and rotation speed on S and P were investigated. Finally, the mixing performance of the dynamic mixer was compared with that of SK and SX static mixers.

2. THE STRUCTURAL DESIGN AND NUMERICAL METHODS

2.1 Structural Design

The dynamic mixer mounted on the co-extruder was driven by a servo motor (Fig. 1 (a) and (b)). In the dynamic mixer, the melt flows through three zones of entrance, mixing, and exit in turn.

In the entrance zone, the melt flows around the rotating shaft, with an annular-shaped cross-section. In the mixing zone, the melt is dispersed and mixed by a rotating cone-shaped rotor with a skirt (height of 3 mm and thickness of 2 mm), on which there are 26 holes (with a diameter of 2 mm) distributed uniformly. In the exit zone, the melt forms a cylindrical flow restricted by exit dimensions. L_i, g, and d_2 were selected for optimization. Based on existing literature (Xu et al., 2013) regarding the high shear mixer, the value range of g was set to 1 to 1.5 mm, that of L_i was set to 0.5 to 1.5D_i, and that of d_2 was set to 1.5 to 2D_i, where D_i was 16 mm. Table 1 shows the levels and values of L_i, g, and d_2. The other dimensions are constant and directly marked in Fig. 1(b).

Table 1 Factors and levels.

Level	Factor		
	L_i, mm	g, mm	d_2, mm
I	8	1	24
II	16	1.25	28
III	24	1.5	32

The diameter of the shaft in the entrance zone (d_i) is the most important parameter for the strength and life of the dynamic mixer. According to the Mechanical Design Manual (Chen, 2016), d_i was calculated using Eq. (1) and was approximately equal to 11 mm.

$$d_i = 17.2\left(\frac{T}{\tau_p}\right)^{1/3} \tag{1}$$

Where T denotes the operating torque (10 N·m), and τ_p stands for the required torsional shear stress (45 MPa).

For comparison, the SK and SX static mixers with the same inlet and outlet dimensions (D_i, L_i, D_o, and L_o) were designed to conduct the mixing process (Fig. 1(c and d)). The SK static mixer consists of twisted blades at 180°. Blades with different rotation directions (left or right-handed) are arranged crosswise and alternately. The SX static mixer is composed of cross blades that are perpendicular to each other, and the angle between the blade and shaft is 45°. Both the thicknesses of the blades of SK and SX static mixers are 1 mm. The lengths of the mixing zone (L_m) of SK and SX static mixers are 84 and 60 mm, and the corresponding number of units is 7 and 5, respectively.

2.2 Mesh

The models of melts, rotor, and static mixers were constructed using the Solidworks2016 software, and then they were divided into unstructured tetrahedral mesh with the same node density in the x, y, and z directions by using the Workbench 19.1 software (Figs. 2-3). Moreover, the

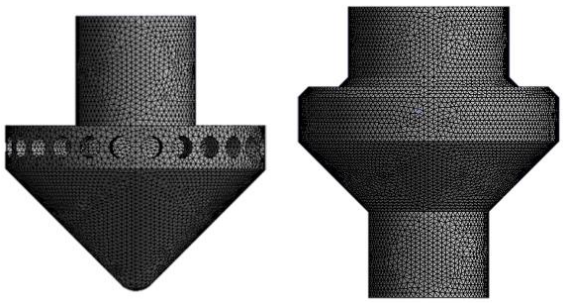

Fig. 2. Grids of the rotor and melt.

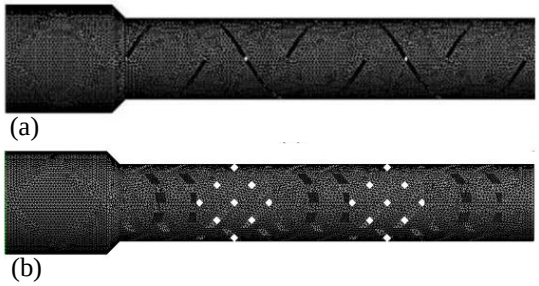

(a)

(b)

Fig. 3. Grids of (a) SK static mixer, and (b) SX static mixer.

Table 2 Grid independent checking.

Side length, mm	Δp, Mpa	Relative deviation
0.43	2.31	0.4%
0.45	2.32	
0.47	2.31	
0.5	2.32	
0.55	2.71	18.4%
0.6	2.89	
0.7	2.44	

grid overlapping technology of Polyflow19.1 (Rathod & Kokini, 2013) was utilized to deal with the relationship between grids of melt and rotor. To obtain a reasonable mesh density, which not only minimizes the effect of mesh on the result but also does not consume too much time of calculation, the side length of the grid is selected in turn from 0.7 to 0.43 mm, and the Δp is computed and evaluated before the formal simulation (Table 2). While changing the side length in the range from 0.7 to 0.55 mm, the Δp varied from 2.89 to 2.44 MPa, with a relative deviation of 18.4%. However, while changing the side length in the range from 0.5 to 0.43 mm, the Δp varied from 2.32 to 2.31 MPa, with a relative deviation of only 0.4%.

It is observed that when the side length is smaller than 0.5 mm, the grid is independent of the result. Therefore, all the models were divided into some grids with a side length of 0.5 mm finally. The more detailed specifications of the grids are presented in Table 3.

2.3 Governing Equations

The melt flow in the mixer was assumed as follows (Meng et al., 2020):

1) The melt was assumed an incompressible non-Newtonian fluid.

2) The melt was presumed to be in a stable laminar flow state, and the entire flow channel was assumed to be filled with the melt.

3) The melt was presumed to have a high viscosity, and gravity and inertial forces were neglected.

4) Density, thermal conductivity, and heat capacity all were assumed constant.

According to the above assumptions, Eqs. (2-5) were used to describe the continuity equation, momentum equation, and heat transfer equation of melt flow (Ishikawa et al., 2000; Zhuang et al., 2020).

$$\nabla \cdot v = 0 \tag{2}$$

$$-\nabla p + \nabla \cdot \tau = 0 \tag{3}$$

$$\rho C_p v \cdot \nabla T_t = k\nabla^2 T_t + \tau : \nabla v \tag{4}$$

$$\tau = 2\eta D \tag{5}$$

Where v stands for the velocity vector (m/s), p is the pressure (Pa), τ is the extra-stress tensor (Pa), T_t is the temperature (°C), η is the viscosity (Pa·s), D is the rate of deformation tensor (s^{-1}), k is the thermal conductivity (0.7 w/(m·K)), ρ is the melt density (920 kg/m^3), and C_p is the specific heat capacity (2000 J/(kg·K)). The other material parameters of Low-Density Polyethylene (LDPE) used in the simulation can be found in the manual of Ansys (2019). The relationship between viscosity and shear rate is represented by the Bird-Carreau model. The relationship between viscosity and temperature is corrected using the approximate Arrhenius model（Eqs. 6-7) (Migliozzi et al., 2021).

Table 3 Detailed specifications of the grids

Name	Side length, mm	Number of grids	Nodes	Element quality	Orthogonal quality	Skewness
The melt in dynamic mixer	0.5	393322	563404	0.8449	0.7825	0.2156
The Rotor of dynamic mixer	0.5	328355	461475	0.8461	0.7852	0.2133
The melt in SK static mixer	0.5	958526	1352699	0.8473	0.7852	0.2131
The melt in SX static mixer	0.5	871407	1272519	0.8387	0.7731	0.2253

$$\eta' = \eta_\infty + (\eta_0 - \eta_\infty)(1 + \lambda^2\dot{\gamma}^2)^{\frac{N-1}{2}} \quad (6)$$

$$\eta(T_t) = \eta' e^{[-\alpha(T_t - T_\alpha)]} \quad (7)$$

Where η_∞ is the viscosity at an infinite shear rate (0 Pa·s), η_0 is the viscosity at a zero shear rate (5699 Pa·s), λ is the relaxation time (0.1 s), $\dot{\gamma}$ is the shear rate (s^{-1}), N is the power-law index (0.33), α is the viscosity-temperature coefficient of the melt (0.015 $℃^{-1}$), and T_α is the reference temperature (473 K).

The shear rate can disperse and decompose solid and liquid agglomerates, thus, a high shear rate represents a good mixing effect (Meng et al., 2017). A more detailed description and more calculation formulas for shear rate can be found in the literature (Ansys, 2019).

2.4 Boundary Conditions and Simulation Method

The boundary conditions were applied as follows: the temperature of the inlet and wall was 200 ℃. The flow rate of the melt at the inlet was 15, 30, and 45 mL/min, and the pressure at the outlet was 0.1 MPa. The rotation speed (n) of the rotor was 120, 180, 240, 300, and 360 r/min. There was no slip between the melt and the wall, thus, the velocity of the melt near the wall was equal to 0, and the velocity of the melt near the rotor was equal to that of the rotor. The time step of the dynamic simulation was the time required for the rotor rotation of 90°. The detailed time steps for the different rotation speeds are presented in Table 4.

The melt flow in the mixer was calculated using the Polyflow software. The Picard interpolation method was employed to calculate the melt viscosity (Proinov, 2010), and the implicit Euler method was selected to solve the equations (Meng et al., 2014; Haddadi et al., 2020). The convergence accuracy was 10^{-4}.

1000 tracer particles of different colors were added on the left and right cross sections at the inlet (Fig. 4) to characterize the mixing effect.

Table 4 Time steps for different rotation speed

n, r/min	Time step, s
120	0.1250
180	0.08333
240	0.06250
300	0.05000
360	0.04167

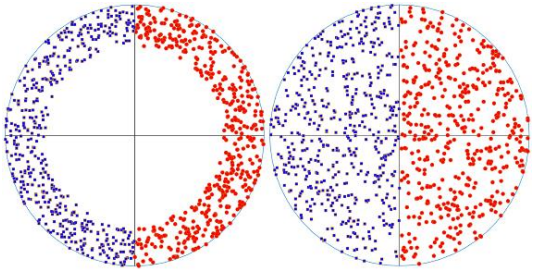

(a) (b)

Fig. 4. Distribution of tracer particles on inlet of (a) Dynamic mixer, and (b) Static mixer.

2.5 Mathematical Calculations

The pressure (p), the shear rate of melt, and the torque on the rotor (T) were acquired via mathematical calculations. The positions of Pr_1, Pr_2, Pr_3, and Pr_4 (see Fig. 1) were selected to observe the p, and the segregation scale (S), which was utilized to characterize the distribution of mixing of the melt, was calculated using Eqs. (8-9) (Connelly & Kokini, 2007).

$$S = \int_0^{\xi} (R|r|)\, d|r| \quad (8)$$

$$R(|r|) = \frac{\sum_{j=1}^{m}(C_j' - \bar{C})(C_j'' - \bar{C})}{m\sigma^2} \quad (9)$$

Where $R(|r|)$ is the Euler correlation coefficient between the concentrations of pairs of points separated by distance $|r|$, σ^2 is the sample variance, m is the number of the pairs of points separated by $|r|$, C_j' and C_j'' are the concentrations of two points in the jth pair, and $\bar{C}$ stands for the average concentration.

The pressure drop (Δp) was calculated using Eq. (10).

$$\Delta p = |p_i - p_o| \quad (10)$$

Where p_i and p_o are the average pressures at the inlet and outlet locations, respectively.

Power consumption refers to the total energy consumed in unit time (Kowalski, 2009), which was calculated by Eq. (11) as follows:

$$P = P_T + P_F + P_L = \Delta p \cdot Q + \frac{n \cdot T}{9.55} + P_L \quad (11)$$

Where P_T is the power consumed by the rotor to overcome the fluid resistance during rotation, P_F is the power loss caused by fluid flowing through the mixer, and P_L is the power loss caused by kinetic power loss, noise, vibration, and other factors at the inlet and outlet. We did not consider the influence of P_L, so P_L=0. Q is the volume flow rate (mL/min), n is the rotation speed (r/min), and T is the torque (N·m).

2.6 Orthogonal Experiment and Results Analysis

The Orthogonal experiment L_9 (3^4) with three factors (L_i, g, d_2) and three levels (see Table 1) was designed to optimize the dynamic mixer. Range analysis and Analysis of Variance (ANOVA) were employed to analyze the influencing order of the factors on Δp, S, T, P, and $S{\cdot}P$. The dynamic mixer with the optimum parameters (L_i, g, d_2) for the minimum $S{\cdot}P$ was chosen to further investigate the influence of flow rate and rotation speed on mixing effect and power consumption. Ultimately, the mixing property and power consumption of dynamic mixer, and SK and SX static mixers were compared.

3. RESULTS AND DISCUSSION

3.1 Orthogonal Experiment Results

The Orthogonal experiment results are presented in Table 5. The influence order of each factor on the results of Δp, S, T, P, and $S{\cdot}P$ can be obtained through the range analysis. The significance of each factor for the results can be obtained through ANOVA.

Table 5 L_9 (3^4) Orthogonal experiment scheme and results

Test serial number	Factor			Results				
	L_i	g	d_2	Δp, MPa	S, μm	T, N·m	P, W	S·P, μm·W
1	1	1	1	2.151	109.9	1.076	28.11	3089
2	1	2	2	1.601	142.3	1.677	42.94	6108
3	1	3	3	1.089	127.7	2.484	62.98	8038
4	2	1	2	2.439	32.65	1.721	44.47	1452
5	2	2	3	1.741	45.70	2.597	66.13	3022
6	2	3	1	1.250	125.1	1.284	32.90	4116
7	3	1	3	2.838	27.18	2.692	69.07	1877
8	3	2	1	1.877	97.90	1.416	36.53	3576
9	3	3	2	1.421	127.8	1.947	49.63	6342
10 (optimization)	2	1	1	2.316	32.58	1.247	32.50	1059

Table 6 Results of Range analysis

		L_i	g	d_2
Δp	k_1	1.614	2.476	1.759
	k_2	1.810	1.740	1.820
	k_3	2.045	1.253	1.889
	R	0.4310	1.223	0.1300
S	k_1	126.6	56.58	111.0
	k_2	67.82	95.28	100.9
	k_3	84.29	126.9	66.84
	R	58.78	70.32	44.16
T	k_1	1.746	1.830	1.259
	k_2	1.867	1.897	1.781
	k_3	2.018	1.905	2.591
	R	0.2720	0.07500	1.332
P	k_1	44.68	47.22	32.51
	k_2	47.83	48.53	45.68
	k_3	51.74	48.50	66.06
	R	7.060	1.310	33.55
S·P	k_1	5745	2140	3594
	k_2	2863	4236	4634
	k_3	3932	6166	4313
	R	2882	4026	1040

3.2 Range Analysis

Table 6 displays the results of the range analysis. The importance orders of influencing the results of Δp and S are the same (for both $g > L_i > d_2$), But the schemes for the minimum Δp and S are different. For the former, it is L_i1g3d_21, and for the latter, it is L_i2g1d_23. It can be concluded that g, as the most important factor, has an opposite impact on the Δp and S. The larger g, the smaller Δp. On the contrary, the larger g, the larger S.

The importance orders of influencing T and P are the same (for both $d_2 > L_i > g$). Moreover, both the level combinations for the minimum T and P are L_i1g1d_21.

The importance order that influences S·P is $g > L_i > d_2$, and the factor level combination for the minimum S·P is L_i2g1d_21, which represents L_i of 16 mm, g of 1 mm, and d_2 of 24 mm. The corresponding value of S·P is 1059 μm·W, (see the test serial number 10 (optimization) in Table 5).

3.3 ANOVA

The results of the Orthogonal experiment were analyzed using ANOVA to identify whether the factors were influential on response results (Table 7). When F-value was smaller than 19, the confidence level was not significant (-). When F-value was greater than 19 and smaller than 99, the confidence level was significant (*). And when F-value was greater than 99, the confidence level was more significant (**) (Minitab, 2021).

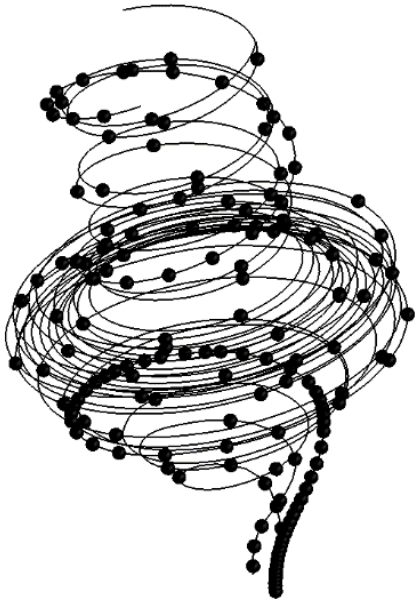

Fig. 5. Path of the particles in the dynamic mixer (flow rate=30 mL/min and n=240 r/min).

For Δp, the F-values of L_i, g, and d_2 were 10.90, 88.56, and 0.9837, respectively. The g was the most significant and important factor, followed by L_i and d_2, which were not significant factors. These findings were consistent with the results of the range analysis.

For S·P, the F-values of factors L_i, g, and d_2 were 80.11, 153.0, and 10.71, respectively. Because the F-value of g was greater than 99, it indicated that g was more significant (**). The F-value of L_i was between 19 and 99, so L_i was significant (*). The F-value of d_2 was smaller than 19, suggesting that d_2 had no significant impact on S·P. These findings were also consistent with the range analysis.

For S, T, and P, the results from ANOVA were also consistent with the results of the range analysis.

Table 7 Results of ANOVA

Source		L_i	g	d_2	Error	Total
df		2	2	2	2	8
Δp	Adj. *SS*	0.2800	2.275	0.02527	0.02569	2.606
	F-value	10.90	88.56	0.9837		
	Level of significance	-	*	-		
S	Adj. *SS*	5517	7433	3208	231.0	16389
	F-value	23.89	32.18	13.89		
	Level of significance	*	*	-		
T	Adj. *SS*	0.1120	0.01022	2.703	0.0002420	2.826
	F-value	461.8	42.14	11150		
	Level of significance	**	*	**		
P	Adj. *SS*	75.23	3.367	1714	0.2213	1793
	F-value	340.0	15.21	7745		
	Level of significance	**	-	**		
S·P	Adj. *SS*	12737107	24325480	1702772	158987	38924346
	F-value	80.11	153.0	10.71		
	Level of significance	*	**	-		

note: *F*- critical value of significance levels * and ** are 19 and 99, respectively.

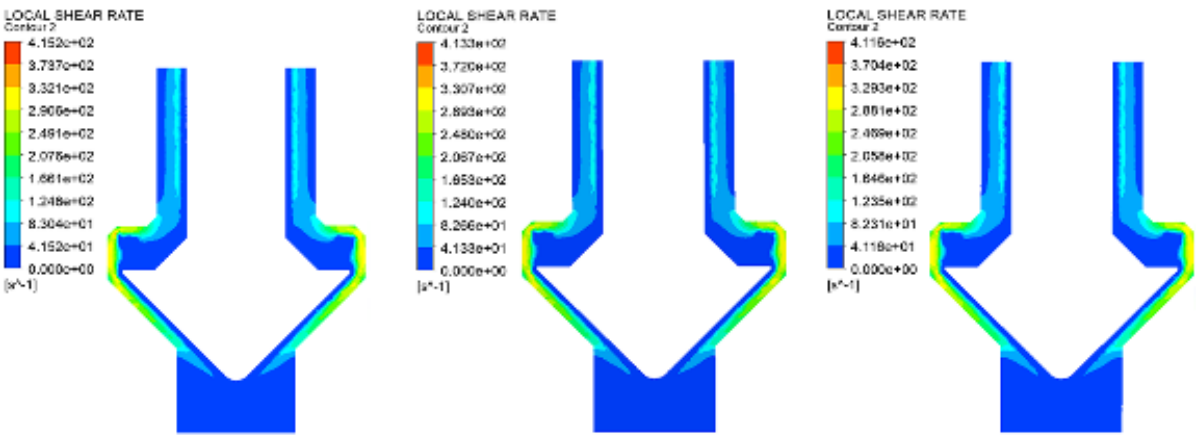

(a) (b) (c)

Fig. 6. Shear rate of melt in the dynamic mixer with *n* of 240 r/min and flow rate of (a) 15, (b) 30, and (c) 45 mL/min.

3.4 The results of the Flow Field

The path of particles from the inlet to the outlet in the dynamic mixer is shown in Fig. 5. The particles first enter the entrance zone and undergo a simple rotary mixing, then enter the mixing zone and experience high shear and dispersion. Finally, particles enter the exit zone and flow out in the form of a cylindrical steady state.

Figure 6 depicts the contour of the shear rate of the melt in the dynamic mixer. The maximum shear rates observed in the mixing zone were 415.2, 413.3, and 411.6 s^{-1} respectively, at the flow rates of 15, 30, and 45 mL/min. The 100% and 200% increases in flow rate were associated with less than 0.5% and 1% changes in shear rate. It can be concluded that the flow rate had little impact on the shear rate of the melt in the dynamic mixer.

Figure 7 exhibits the pressures at the positions of Pr_1, Pr_2, Pr_3, and Pr_4 under different flow rates. With moving from position Pr_1 to Pr_4, the pressure showed a downward trend. The pressure was greatly affected by the flow rate.

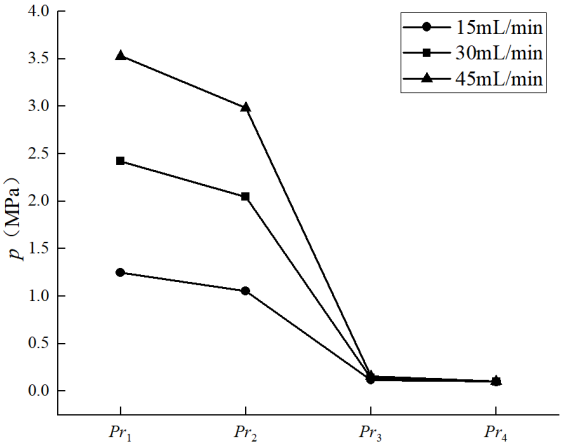

Fig. 7. Pressure profile along the flow direction with *n* of 240 r/min.

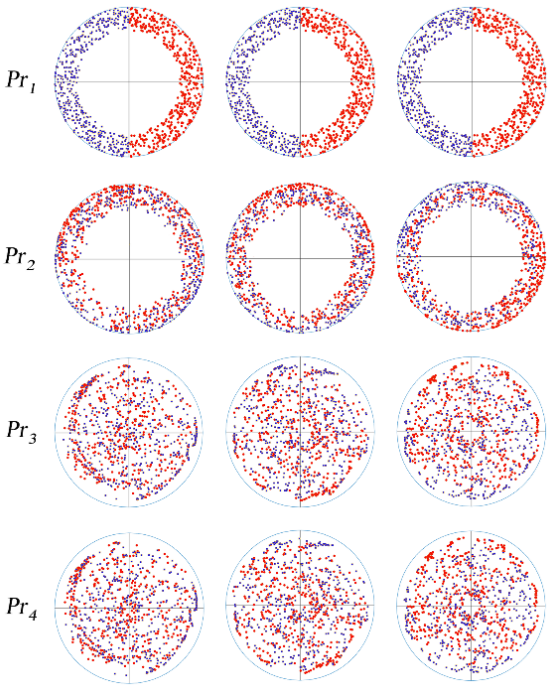

Fig. 8. Particles distribution along flow direction with *n* of 240 r/min and flow rate of (a) 15, (b) 30, and (c) 45 mL/min.

When the flow rate increased from 15 mL/min to 30 and 45 mL/min (a 100% and 200% increase, respectively), the corresponding pressure of Pr_1 increased from 1.25 MPa to 2.42 and 3.53 MPa, reflecting a 94% and 182% increase, respectively.

The distribution of tracer particles was different at different positions (Fig. 8). In the entrance zone, the particles were preliminarily rotated and mixed. In the mixing zone, the particles were further mixed with high shear. The most uniform distribution was observed in position Pr_4.

Furthermore, we found that the larger the flow rate, the worse the mixing effect. At position Pr_4, the *S* from the flow rate of 15, 30, and 45 mL/min was 19, 32, and 111 μm, respectively. More agglomerations of particles were observed in the results of the larger flow rates of 30 and 45 mL/min. This was because the increase in flow rate decreased the residence time of the melt in the dynamic mixer. The shorter residence time led to the shorter and weaker effect of the rotor on the melt, thus, the worse mixing results were observed under the larger flow rates.

3.5 The effect of Rotation Speed on *S* and *P*

Figure 9 shows that the *S* decreases and *P* increases with the increase of rotation speed. Thus, the desired *S* can be obtained by controlling the rotation speed. When the flow rate was 15 mL/min, the *S* could be diminished to 33 μm by imposing a rotation speed larger than 226.5 r/min, and the corresponding *P* was 29 W. When the flow rate was 30 mL/min, the required rotation speed for reducing *S* to 33 μm was 240 r/min, and the corresponding *P* was 33 W. This suggested that if the flow rate is increased to 100%, the *P* required to achieve the same *S* will increase

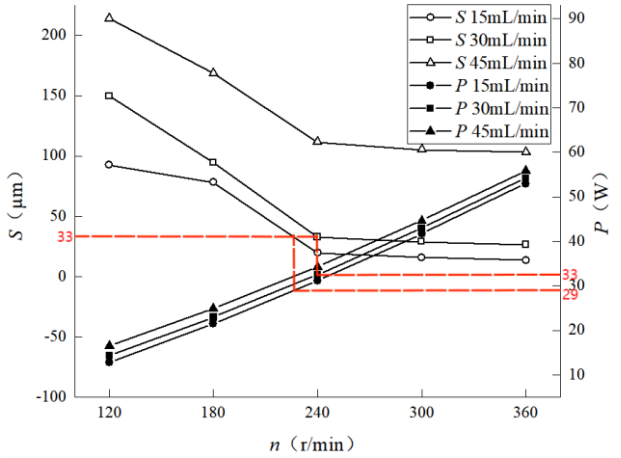

Fig. 9. *S* and *P* changing with the rotation speed.

by 37.5%. Furthermore, when the flow rate increased to 45 mL/min, the *S* could not be reduced to 33 μm, despite using the highest rotation speed (360 r/min). The minimum *S* of 12 μm was obtained in the dynamic mixer when the flow rate was 15 mL/min and the rotation speed was 360 r/min, and the corresponding *P* was 53 W.

3.6 Comparison with Static Mixer

With the increase in the length of the static mixer, the *S* decreases and *P* increases monotonically (Fig. 10). We also found that in the range from 15 to 45 mL/min, the larger the flow rate, the larger the *P* and *S*. The *S* of SX static mixer was smaller than that of SK static mixer, and the *P* of the former was larger than that of the latter, with the same length.

When the flow rate was 30 mL/min, the *P* required to achieve the *S* of 33 μm was 2.8 W for SK static mixer, 11 W for SX static mixer, and 33 W for the dynamic mixer. This means that for achieving the same *S*, the *P* of the dynamic mixer is the largest, and that of the SK static mixer is the smallest. The same conclusion was drawn when the flow rate was 15 and 45 mL/min.

The needed length for obtaining the *S* of 33 μm was 84 mm for SK static mixer, 60 mm for SX static mixer, and 16 mm for the dynamic mixer. Therefore, the length of the SK static mixer was the longest, and that of the dynamic mixer was the shortest. Similar results could be obtained when the flow rate was 15 and 45 mL/min.

The minimum *S* of 22 and 13 μm was observed for SK and SX static mixers, respectively, and the corresponding *P* was 0.89 and 6.3 W. It can be concluded that although the larger *P* is needed for the dynamic mixer, a better mixing effect is achieved using the dynamic mixer compared with SK and SX static mixers.

4. CONCLUSION

An online dynamic mixer was designed to perform the mixing for polymer melts. The mixing properties of the dynamic mixer were analyzed and optimized and compared with those of SK and SX static mixers. The main findings of this research are as follows:

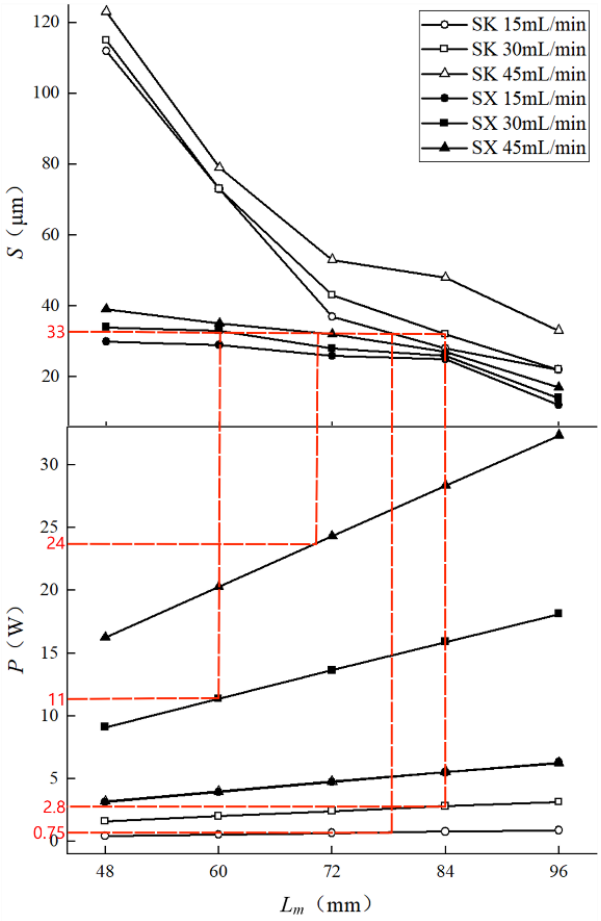

Fig. 10. *S* and *P* varying with the length of SK and SX static mixers.

- Using the designed dynamic mixer, the mixing effect of the polymer melt can be regulated online without changing the flow rate. It is not possible with screw mixers and static mixers.
- The *g* was the most significant factor influencing *S*·*P* of the dynamic mixer. When the values of L_i, *g*, and d_2 were 16, 1, and 24 mm respectively, the minimum *S*·*P* was attained. The maximum of shear rate of 415.2 s^{-1} was observed in the mixing zone of the dynamic mixer and it was less affected by the flow rate.
- In the dynamic mixer, *P* increased with the increase of both the flow rate and rotation speed. The *S* increased with the increase of the flow rate from 15 to 45 mL/min, and decreased with the increase of rotation speed from 120 to 360 r/min. The minimum *S* of 12 μm was obtained with the smallest flow rate of 15 mL/min and the largest rotation speed of 360 r/min.
- To achieve the same *S*, the length of the dynamic mixer was the shortest, and that of the SK static mixer was the longest. The dynamic mixer consumed the largest *P*, SX static mixer consumed a smaller *P*, and SK static mixer consumed the smallest *P*.

ACKNOWLEDGEMENTS

The authors would like to express their gratitude to all contributors for their technical support and EditSprings for the expert linguistic services.

CONFLICT OF INTEREST

The authors declare that they have no known competing financial interests or personal relationships that could have appeared to influence the work reported in this paper.

AUTHORS CONTRIBUTION

Y. W. Zheng performed the data analyses and wrote the manuscript; J. K. Wang contributed significantly to analysis and manuscript preparation; J. G. Sun helped perform the analysis with constructive discussions; C. Y. Wang contributed to the conception of the study.

REFERENCES

Ansys (2019). *POLYFLOW 19.1 User's Guide*.

Bauer, H., & Khinast, J. (2022). Detecting mixing barriers in twin screw extruder elements via lagrangian coherent structures. *Chemical Engineering Science*, 263, 1-13. https://doi.org/10.1016/j.ces.2022.118069

Cai, R. H., Hou, Z. C., & Zhao, Y. Z. (2019). Numerical study on particle mixing in a double-screw conical mixer. *Powder Technology*, 352, 193-208. https://doi.org/10.1016/j.powtec.2019.04.065

Carcia, B. E., Zacarias, A., Ferrer, V. H., & Vargas, R. O. (2018). Numerical simulation of the Non-isothermal co-extrusion fiber spinning with flow-induced crystallization. *Journal of Applied Fluid Mechanics*, 11(5), 1207-1215. https://doi.org/10.18869/acadpub.jafm.73.248.28323

Carolina, C. M., Maria, D., Mohanadmandi, S., Carlos, F., Enda, J., Christian, M., Suanshine, H., Norma, A., Ali, A., & Ivonne, G. (2020). Using chaotic advection for facile high-throughput fabrication of ordered multilayer micro- and nanostructures: continuous chaotic printing. *Biofabrication*, 12(3), 035023. https://doi.org/10.1088/1758-5090/ab84cc

Chen, D. X. (2016). *Handbook of mechanical design (Fifth Edition)*. The book.

Chen, H., Guo, M., Schiraldi, D., & Maia, J. M. (2021). Morphology optimization of poly (ethylene terephthalate)/polyamide blends compatibilized via extension-dominated twin-screw extrusion. *Journal of Polymer Engineering*, 41(3), 218-225. https://doi.org/10.1515/polyeng-2020-0229

Common, A., Rodier, E., Sauceau, M., & Fages, J. (2014). Flow and mixing efficiency characterization in a CO_2-assisted single-screw extrusion process by residence time distribution using raman spectroscopy. *Chemical Engineering Research and Design*, 92(7), 1210-1218. https://doi.org/10.1016/j.cherd.2013.10.013

Connelly, R. K., & Kokini, J. L. (2007). Examination of the mixing ability of single and twin screw mixers using 2D finite element method simulation with particle tracking. *Journal of Food Engineering*, 79(3), 956–969. https://doi.org/10.1016/j.jfoodeng.2006.03.017

Eriksson, M., Meuwissen, M., Peijs, T., & Goossens, H. (2020). The Influence of Melt-Mixing Conditions and State of Dispersion on Crystallisation, Rheology and Mechanical Properties of PCL/Sepiolite Nanocomposites. *International Polymer Processing*, 35(3), 302-313. https://doi.org/10.3139/217.3890

Haddadi, M. M., Hosseini, S. H., Rashtchian, D., & Olazar, M. (2019). Comparative analysis of different static mixers performance by CFD technique: An innovative mixer. *Chinese Journal of Chemical Engineering*, 28(3), 672-684. https://doi.org/10.1016/j.cjche.2019.09.004

Ishikawa, T., Kihara, S. I., & Funatsu, K. (2000). Numerical simulation and experimental verification of nonisothermal flow in counter-rotating nonintermeshing continuous mixers. *Polymer Engineering and Science*, 40(2), 365-375. https://doi.org/10.1002/pen.11170

Jian, R. R., Yang, W. M., Cheng, L. S., & Xie, P. C. (2018). Numerical simulation on the enhanced mixing of polymer melt by single screw with torsion elements in the homogenizing section. *Polymer-Korea*, 42(6), 910-918. https://doi.org/10.7317/pk.2018.42.6.910

Kowalski, A. J. (2009). An expression for the power consumption of in-line rotor-stator devices. *Chemical Engineering and Processing: Process Intensification*, 48(1), 581–585. https://doi.org/10.1016/j.cep.2008.04.002

Lin, C. M., & Chang, Y. W. (2021). Optimization designation of static mixer geometry considering mixing effect. *Microsystem Technologies-micro-and Nanosystems-information Storage and Processing Systems*, 27(3), 883-892. https://doi.org/10.1007/s00542-020-04962-y

Liu, J., & Zhu, X. Z. (2019). Chaotic mixing analysis of a novel single-screw extruder with a perturbation baffle by the finite-time Lyapunov exponent method. *Journal of Polymer Engineering*, 39(3), 287-299. https://doi.org/10.1515/polyeng-2018-0037

Minitab (2021). *Minitab Statistical Software*.

Meng, H. B., Wang, F., Yu, Y., Song, M., & Wu, J. (2014). A Numerical Study of Mixing Performance of High-Viscosity Fluid in Novel Static Mixers with Multitwisted Leaves. *Industrial & Engineering Chemistry Research*, 53(10), 4084–4095. https://doi.org/10.1021/ie402970v

Meng, H. B., Jiang, X. H., & Yu, Y. F. (2017). Laminar flow and chaotic advection mixing performance in a static mixer with perforated helical segments. *Korean Journal of Chemical Engineering*, 34(5), 1328-1336. https://doi.org/10.1007/s11814-017-0035-z

Meng, H. B., Han, M. Q., & Yu, Y. F. (2020). Numerical evaluations on the characteristics of turbulent flow and heat transfer in the Lightnin static mixer. *International Journal of Heat and Mass Transfer*, 156, 119788. https://doi.org/10.1016/j.ijheatmasstransfer.2020.119788

Migliozzi, S., Mazzei, L., & Angeli, P. (2021). Viscoelastic flow instabilities in static mixers: Onset and effect on the mixing efficiency. *Physics of Fluids*, 33(1), 013104. https://doi.org/10.1063/5.0038602

Marschik, C., Osswald, T. A., Roland, W., Albrecht, H., Skrabala, O., & Miethlinger, J. (2019). Numerical analysis of mixing in block-head mixing screws. *Polymer Engineering and Science*, 59, E88-E104. https://doi.org/10.1002/pen.24968

Proinov, P. D. (2010). New general convergence theory for iterative processes and its applications to Newton–Kantorovich type theorems. *Journal of Complexity*, 26(1), 3–42. https://doi.org/10.1016/j.jco.2009.05.001

Rathod, M. L., & Kokini, J. L. (2013). Effect of mixer geometry and operating conditions on mixing efficiency of a non-Newtonian fluid in a twin screw mixer. *Journal of Food Engineering*, 118(3), 256–265. https://doi.org/10.1016/j.jfoodeng.2013.04.020

Robinson, M., & Cleary, P. W. (2019). Effect of geometry and fill level on the transport and mixing behaviour of a co-rotating twin screw extruder. *Computational Particle Mechanics*, 6(2), 227-247. https://doi.org/10.1007/s40571-018-0210-y

Rochman, A., & Zahra, K. (2018). Development and performance analysis of static mixing nozzle for injection molding of thermoset elastomers. *Polymer Engineering and Science*, 58(4), 521-527. https://doi.org/10.1002/pen.24763

Talhaoui, A., Draoui, B., & Youcefi, A. (2021). Effect of geometry design on mixing performance of newtonian fluid using helical overlapped mixer elements in kenics static mixer. *Journal of Applied Fluid Mechanics*, 14 (6), 1643-1656. https://doi.org/10.47176/jafm.14.06.32494

Varga, A., Keppler, I., & Fenyvesi, L. (2020). Determination the efficiency of open mixing screws. *Journal of Mechanical Science and Technology*, 34(6), 2327-2332. https://doi.org/10.1007/s12206-020-0508-6

Xu, B. P., Liu, Y., He, L., Chen, J. W., & Turng, L. S. (2018). Numerical study of mixing dynamics inside the novel elements of a corotating nontwin screw extruder. *Advances in Polymer Technology*, 37(7), 2478-2496. https://doi.org/10.1002/adv.21923

Xu, S., Shi, J., Cheng, Q., Li, W., & Zhang, J. (2013). Residence time distributions of in-line high shear mixers with ultrafine teeth. *Chemical Engineering Science*, 87, 111–121. https://doi.org/10.1016/j.ces.2012.10.017

Zhuang, Z. K., Yan, J. T., & Sun, C. L. (2020). The numerical simulation of a new double swirl static mixer for gas reactants mixing. *Chinese Journal of Chemical Engineering*, 28(9), 2438-2446. https://doi.org/10.1016/j.cjche.2020.05.008